

Open Charm Production in an Equilibrating Parton Plasma

Peter Lévai^a, Berndt Müller^b, and Xin-Nian Wang^c

^a*Research Institute for Particle and Nuclear Physics,*

H-1525 Budapest 114, P. O. Box 49, Hungary

^b*Department of Physics, Duke University,*

Durham, NC 27708-0305

^c*Nuclear Science Division, MS 70A-3307,*

Lawrence Berkeley Laboratory, Berkeley, CA 94720

(November 21, 1994)

Abstract

Open charm production during the equilibration of a gluon dominated parton plasma is calculated, with both the time-dependent temperature and parton densities given by a set of rate equations. Including pre-thermal production, the total enhancement of open charm production over the initial gluon fusion depends sensitively on the initial parton density and the effective temperature. The dependence of the pre-thermal charm production on the space-momentum correlation in the initial parton phase-space distribution is also discussed.

25.75.+r, 12.38.Mh, 13.87.Ce, 24.85.+p

I. INTRODUCTION

At extremely high energies, nucleus-nucleus collisions may be described by parton interactions in the framework of perturbative QCD (pQCD)-inspired models [1–3]. In this framework, hard or semihard scatterings among partons dominate the reaction dynamics. They can liberate partons from the individual confining nucleons, thus producing large amount of transverse energy in the central region [4,5], and drive the initially produced parton system toward equilibrium [2,6–8]. In principle, the same kind of hard processes, such as open charm production [9–11], direct photon and dilepton production [12,13], can also be used as direct probes of the early parton dynamics and the evolution of the quark-gluon plasma. Unlike strange quarks, charm quarks cannot be easily produced during the mixed and hadronic phases of the dense matter since the charm mass is much larger than the corresponding temperature scale. The only period when charm quarks can be easily produced is during the early stage of the parton evolution when the effective temperature is still high. At this stage, the parton gas is still not fully equilibrated yet so that the temperature is only an effective parameter describing the average momentum scale. By measuring this pre-equilibrium charm production, one can thus probe the initial parton density in phase space and shed light on the equilibration time [9].

Roughly speaking, ultrarelativistic heavy-ion collisions in a partonic picture can be divided into three stages: (1) During the early stage, hard or semihard parton scatterings, which happen on a time scale of about $0.2 \text{ fm}/c$, produce a hot and dilute parton gas. This parton gas is dominated by gluons and its quark content is far below the chemical equilibrium value. Multiple hard scatterings suffered by a single parton during this short period of time when the beam partons pass through each other are suppressed due to the interference embedded in the Glauber formula for multiple scatterings [14]. This leads to the observed disappearance of the Cronin effect at high energy and at large transverse momentum [15]. Interference and parton fusion also lead to the depletion of small- x partons in the effective parton distributions inside a nucleus [16,17]. This nuclear shadowing of parton

distributions reduces the initial parton production [18]. (2) After two beams of partons pass through each other, the produced parton gas in the central rapidity region starts its evolution toward (kinetic) thermalization mainly through elastic scatterings and expansion. The kinematic separation of partons through free-streaming gives an estimate of the time scale $\tau_{\text{iso}} \sim 0.5 - 0.7 \text{ fm}/c$ [7,19], when local isotropy in momentum distributions is reached. (3) Further evolution of the parton gas toward a fully (chemically) equilibrated parton plasma is dictated by the parton proliferation through induced radiation and gluon fusion. Due to the consumption of energy by the additional parton production, the effective temperature of the parton plasma cools down considerably faster than the ideal Bjorken's scaling solution. Therefore, the life time of the plasma is reduced before the temperature drops below the QCD phase transition temperature [7].

Similarly, charm production can also be divided into three different contributions in the history of the evolution of the parton system: (1) initial production during the overlapping period ; (2) pre-thermal production from secondary parton scatterings during the thermalization, $\tau < \tau_{\text{iso}}$; (3) and thermal production during the parton equilibration, $\tau > \tau_{\text{iso}}$, in the expanding system. In this paper, we will first review the equilibration of the initially produced parton gas in Sec. II, incorporating the result of an improved perturbative QCD analysis of Landau-Pomeranchuk-Migdal (LPM) effect [20,21]. Then we will discuss the three stages of open charm production in a reversed order, starting with the charm production during the final stage of parton equilibration in Sec. III. For pre-thermal charm production, we will consider the space-momentum correlation in the initial parton phase-space distributions, which will suppress open charm production during this period as compared to previous estimates [9]. In Sec. IV, we will compare the results to the charm production during the initial hard or semi-hard scatterings and also to the results in Geiger's calculation [10] which is about 40-50 times higher than our estimates here. We will also discuss the change in charm production due to the uncertainties in the initial parton density and effective temperature. Finally we give our conclusions in Sec. V.

II. PARTON PRODUCTION AND EQUILIBRATION

At collider energies ($\sqrt{s} > 100$ GeV), hard or semihard parton scatterings are believed to be the dominant mechanism for transverse energy production in the central region [4,5]. These hard processes happen on a short time scale and they generally break color coherence inside individual nucleons [22]. After the fast parton pass through each other and leave the central region, a partonic gas will be left behind which is not immediately in thermal and chemical equilibrium. The partons inside such a system will then undergo further interactions and free-streaming. Neglecting parton scatterings in this period of time, the kinematic separation of partons with different rapidities in a cell establishes local momentum isotropy at the time of the order of $\tau_{\text{iso}} = 0.7$ fm/ c [7,19]. If we assume this is the actual kinetic equilibration (or thermalization) time for the partonic system, The subsequent chemical equilibration can then be described by a set of rate equations. In this section we will review parton equilibration following Ref. [7] with improved estimate of the gluon equilibration rate.

A. Initial conditions: a hot and dilute gluonic gas

Currently there are many models for incorporating hard and semi-hard processes in hadronic and nuclear collisions [1–3]. We will use the results of the HIJING Monte Carlo model [1] to estimate the initial parton production. In this model, multiple hard or semi-hard parton scatterings with initial and final state radiation are combined together with Lund string phenomenology [23] for the accompanying soft nonperturbative interactions.

Let us first estimate the initial conditions at time, τ_{iso} , from the HIJING results. Since we are here primarily interested in the chemical equilibration of the parton gas which has already reached local isotropy in momentum space, we shall assume that the parton distributions can be approximated by thermal phase space distributions with non-equilibrium fugacities λ_i :

$$f(k; T, \lambda_i) = \lambda_i \left(e^{u \cdot k/T} \pm \lambda_i \right)^{-1}, \quad (1)$$

where u^μ is the four-velocity of the local comoving reference frame. When the parton fugacities λ_i are much less than unity as may happen during the early evolution of the parton system, we can neglect the quantum corrections in Eq. (1) and write the momentum distributions in the factorized form,

$$f(k; T, \lambda_i) = \lambda_i \left(e^{u \cdot k/T} \pm 1 \right)^{-1}. \quad (2)$$

Using this form of distributions, one has the parton and energy densities,

$$n = (\lambda_g a_1 + \lambda_q b_1) T^3, \quad \varepsilon = (\lambda_g a_2 + \lambda_q b_2) T^4. \quad (3)$$

where $a_1 = 16\zeta(3)/\pi^2 \approx 1.95$, $a_2 = 8\pi^2/15 \approx 5.26$, for a Bose distribution, $b_1 = 9\zeta(3)N_f/\pi^2 \approx 2.20$ and $b_2 = 7\pi^2 N_f/20 \approx 6.9$ for a Dirac distribution. For a baryon symmetric system, $\lambda_q = \lambda_{\bar{q}}$. Since boost invariance has been demonstrated to be a good approximation for the initially produced partons [19], we can then estimate the initial parton fugacities, $\lambda_{g,q}^0$ and temperature T_0 from

$$n_0 = \frac{1}{\pi R_A^2 \tau_{\text{iso}}} \frac{dN}{dy}, \quad \varepsilon_0 = n_0 \frac{4}{\pi} \langle k_T \rangle, \quad (4)$$

where $\langle k_T \rangle$ is the average transverse momentum. The quark fugacity is taken as $\lambda_q^0 = 0.16\lambda_g^0$, corresponding to a ratio 0.14 of the initial quark(antiquark) number to the total number of partons. Table I shows these relevant quantities at the moment τ_{iso} , for Au + Au collisions at Brookhaven National Laboratory Relativistic Heavy Ion Collider (RHIC) and CERN Large Hadron Collider (LHC) energies. One can observe that the initial parton gas is rather hot reflecting the large average transverse momentum. However, the parton gas is very dilute as compared to the ideal gas at the same temperature. The gas is also dominated by gluons with its quark content far below the chemical equilibrium value. We should emphasize that the initial conditions listed here result from HIJING calculation of parton production through semihard scatterings. Soft partons, *e.g.*, due to parton production from the color field [24], are not included.

B. Master rate equations

In general, chemical reactions among partons can be quite complicated because of the possibility of initial and final-state gluon radiations. Interference effects due to multiple scatterings inside a dense medium, *i.e.*, LPM suppression of soft gluon radiation has to be taken into account. One lesson one has learned from LPM effect [20,21] is that the radiation between two successive scatterings is the sum, *on the amplitude level*, of both the initial state radiation from the first scattering and the final state radiation from the second one. Since the off-shell parton is space-like in the first amplitude and time-like in the second, the picture of a time-like parton propagating inside a medium in the parton cascade simulations [2] shall break down. Instead, we shall here consider both initial and final state radiations together associated with a single scattering (To the leading order, a single additional gluon is radiated, such as $gg \rightarrow ggg$), in which we can include LPM effect by a radiation suppression factor. The analysis of QCD LPM effect in Ref. [20,21] has been done for a fast parton traveling inside a parton plasma. We will use the results for radiations off thermal partons who average energy is about T , since we expect the same physics to happen.

In order to permit the approach to chemical equilibrium, the reverse process, *i.e.*, gluon absorption, has to be included as well, which is easily achieved making use of detailed balance. We consider only the dominant process $gg \rightarrow ggg$. Radiative processes involving quarks have substantially smaller cross sections in pQCD, and quarks are considerably less abundant than gluons in the initial phase of the chemical evolution of the parton gas. Here we are interested in understanding the basic mechanisms underlying the formation of a chemically equilibrated quark-gluon plasma, and the essential time-scales. We hence restrict our considerations to the dominant reaction mechanism for the equilibration of each parton flavor. These are just four processes [25]:

$$gg \leftrightarrow ggg, \quad gg \leftrightarrow q\bar{q}. \quad (5)$$

Other scattering processes ensure the maintenance of thermal equilibrium ($gg \leftrightarrow gg$, $gq \leftrightarrow gq$, etc.) or yield corrections to the dominant reaction rates ($gq \leftrightarrow qgg$, etc.).

Restricting to the reactions in Eq. (5) and assuming that elastic parton scatterings are sufficiently rapid to maintain local thermal equilibrium, the evolution of the parton densities is governed by the master equations [7]:

$$\partial_\mu(n_g u^\mu) = \frac{1}{2} \sigma_3 n_g^2 \left(1 - \frac{n_g}{\tilde{n}_g}\right) - \frac{1}{2} \sigma_2 n_g^2 \left(1 - \frac{n_q^2 \tilde{n}_g^2}{\tilde{n}_q^2 n_g^2}\right), \quad (6)$$

$$\partial_\mu(n_q u^\mu) = \frac{1}{2} \sigma_2 n_g^2 \left(1 - \frac{n_q^2 \tilde{n}_g^2}{\tilde{n}_q^2 n_g^2}\right), \quad (7)$$

where $\tilde{n}_i \equiv n_i/\lambda_i$ denote the densities with unit fugacities, $\lambda_i = 1$, σ_3 and σ_2 are thermally averaged, velocity weighted cross sections,

$$\sigma_3 = \langle \sigma(gg \rightarrow ggg)v \rangle, \quad \sigma_2 = \langle \sigma(gg \rightarrow q\bar{q})v \rangle. \quad (8)$$

We have also assumed detailed balance and a baryon symmetric matter, $n_q = n_{\bar{q}}$. If we neglect effects of viscosity due to elastic scattering [24,26], we then have the hydrodynamic equation

$$\partial_\mu(\varepsilon u^\mu) + P \partial_\mu u^\mu = 0, \quad (9)$$

which determines the evolution of the energy density.

For a time scale $\tau \ll R_A$, we can neglect the transverse expansion and consider the expansion of the parton plasma purely longitudinal, which leads to the Bjorken's scaling solution [27] of the hydrodynamic equation:

$$\frac{d\varepsilon}{d\tau} + \frac{\varepsilon + P}{\tau} = 0. \quad (10)$$

We further assume the ultrarelativistic equation of motion, $\varepsilon = 3P$ with n_i and ε given by Eq. (3). We can then solve the hydrodynamic equation,

$$[\lambda_g + \frac{b_2}{a_2} \lambda_q]^{3/4} T^3 \tau = \text{const.} \quad , \quad (11)$$

and rewrite the rate equation in terms of time evolution of the parameters $T(\tau)$, $\lambda_g(\tau)$ and $\lambda_q(\tau)$,

$$\frac{\dot{\lambda}_g}{\lambda_g} + 3\frac{\dot{T}}{T} + \frac{1}{\tau} = R_3(1 - \lambda_g) - 2R_2 \left(1 - \frac{\lambda_g^2}{\lambda_q^2}\right) \quad (12)$$

$$\frac{\dot{\lambda}_q}{\lambda_q} + 3\frac{\dot{T}}{T} + \frac{1}{\tau} = R_2 \frac{a_1}{b_1} \left(\frac{\lambda_g}{\lambda_q} - \frac{\lambda_q}{\lambda_g}\right), \quad (13)$$

where the density weighted reaction rates R_3 and R_2 are defined as

$$R_3 = \frac{1}{2}\sigma_3 n_g, \quad R_2 = \frac{1}{2}\sigma_2 n_g. \quad (14)$$

Notice that for a fully equilibrated system ($\lambda_g = \lambda_q = 1$), Eq. (11) corresponds to the Bjorken solution, $T(\tau)/T_0 = (\tau_0/\tau)^{1/3}$.

C. Parton equilibration rates

To take into account of the LPM effect in the calculation of the reaction rate R_3 for $gg \rightarrow ggg$, we simply impose the LPM suppression of the gluon radiation whose effective formation time τ_{QCD} is much longer than the mean-free-path λ_f of multiple scatterings to each $gg \rightarrow ggg$ process. In the mean time, the LPM effect also regularizes the infrared divergency associated with QCD radiation. However, σ_3 still contains infrared singularities in the gluon propagators. For an equilibrium system one can in principle apply the resummation technique developed by Braaten and Pisarski [28] to regularize the electric part of the propagators, though the magnetic sector still has to be determined by an unknown magnetic screening mass which can only be calculated nonperturbatively [29] up to now. Since we are dealing with a nonequilibrium system, Braaten and Pisarski's resummation may not be well defined. As an approximation, we will use the Debye screening mass [22],

$$\mu_D^2 = \frac{6g^2}{\pi^2} \int_0^\infty k f(k) dk = 4\pi\alpha_s T^2 \lambda_g, \quad (15)$$

to regularize all singularities in both the scattering cross sections and the radiation amplitude.

To further simplify the calculation we approximate the LPM suppression factor in Ref. [20,21] by a θ -function, $\theta(\lambda_f - \tau_{\text{QCD}})$, where

$$\tau_{\text{QCD}} = \frac{C_A}{2C_2} \frac{2 \cosh y}{k_\perp}, \quad (16)$$

is the effective formation time of the gluon radiation in QCD which depends on the second Casimir of the beam parton representation in $SU(3)$, *e.g.*, $C_2 = C_A = 3$ for a gluon. In the previous calculation of the interaction rate [7], this color factor was not taken into account. The modified differential cross section for $gg \rightarrow ggg$ is then,

$$\frac{d\sigma_3}{dq_\perp^2 dy d^2 k_\perp} = \frac{d\sigma_{\text{el}}^{gg}}{dq_\perp^2} \frac{dn_g}{dy d^2 k_\perp} \theta(\lambda_f - \tau_{\text{QCD}}) \theta(\sqrt{s} - k_\perp \cosh y), \quad (17)$$

where the second step-function accounts for energy conservation, and $s = 18T^2$ is the average squared center-of-mass energy of two gluons in the thermal gas. The regularized gluon density distribution induced by a single scattering is [30],

$$\frac{dn_g}{dy d^2 k_\perp} = \frac{C_A \alpha_s}{\pi^2} \frac{q_\perp^2}{k_\perp^2 [(\mathbf{k}_\perp - \mathbf{q}_\perp)^2 + \mu_D^2]}. \quad (18)$$

Similarly, the regularized small angle gg scattering cross is,

$$\frac{d\sigma_{\text{el}}^{gg}}{dq_\perp^2} = \frac{9}{4} \frac{2\pi\alpha_s^2}{(q_\perp^2 + \mu_D^2)^2}. \quad (19)$$

The mean-free-path for elastic scatterings is then,

$$\lambda_f^{-1} \equiv n_g \int_0^{s/4} dq_\perp^2 \frac{d\sigma_{\text{el}}^{gg}}{dq_\perp^2} = \frac{9}{8} a_1 \alpha_s T \frac{1}{1 + 8\pi\alpha_s \lambda_g/9}, \quad (20)$$

which depends very weakly on the gluon fugacity λ_g as compared to the independent one used in a previous study [7]. Using,

$$\int_0^{2\pi} d\phi \frac{1}{(\mathbf{k}_\perp - \mathbf{q}_\perp)^2 + \mu_D^2} = \frac{2\pi}{\sqrt{(k_\perp^2 + q_\perp^2 + \mu_D^2)^2 - 4q_\perp^2 k_\perp^2}}, \quad (21)$$

we can complete part of the integrations and have,

$$R_3/T = \frac{32}{3a_1} \alpha_s \lambda_g (1 + 8\pi\alpha_s \lambda_g/9)^2 \mathcal{I}(\lambda_g), \quad (22)$$

where $\mathcal{I}(\lambda_g)$ is a function of λ_g ,

$$\begin{aligned} \mathcal{I}(\lambda_g) = & \int_1^{\sqrt{s}\lambda_f} dx \int_0^{s/4\mu_D^2} dz \frac{z}{(1+z)^2} \left\{ \frac{\cosh^{-1}(\sqrt{x})}{x\sqrt{[x + (1+z)x_D]^2 - 4x z x_D}} \right. \\ & \left. + \frac{1}{s\lambda_f^2} \frac{\cosh^{-1}(\sqrt{x})}{\sqrt{[1 + x(1+z)y_D]^2 - 4x z y_D}} \right\}, \end{aligned} \quad (23)$$

where $x_D = \mu_D^2 \lambda_f^2$ and $y_D = \mu_D^2/s$. We can evaluate the integration numerically and find out the dependence of R_3/T on the gluon fugacity λ_g . In Fig. 1, R_3/T is plotted versus λ_g for a coupling constant $\alpha_s = 0.3$. The gluon production rate increases with λ_g and then saturates when the system is in equilibrium. Note that in principle one should multiply the phase-space integral by $1/3!$ to take into account of the symmetrization of identical particles in $gg \rightarrow ggg$ as in Ref. [12]. However, for the dominant soft radiation we consider here, the radiated soft gluon does not overlap with the two incident gluons in the phase-space. Thus we only multiply the cross section by $1/2!$ to obtain the equilibration rate.

The calculation of the quark equilibration rate R_2 for $gg \rightarrow q\bar{q}$ is more straightforward. Estimate in Ref. [7] gives,

$$R_2 = \frac{1}{2} \sigma_2 n_g \approx 0.24 N_f \alpha_s^2 \lambda_g T \ln(5.5/\lambda_g). \quad (24)$$

The dashed line in Fig. 1 shows the normalized rate R_2/T for $N_f = 2.5$, taking into account the reduced phase space of strange quarks at moderate temperatures, as a function of the gluon fugacity.

D. Evolution of the parton plasma

With the parton equilibration rates which in turn depend on the parton fugacity, we can solve the master equations self-consistently and obtain the time evolution of the temperature and the fugacities. Shown in Figs. 2 and 3 are the time dependence of T , λ_g , and λ_q for initial conditions listed in Table I at RHIC and LHC energies. We find that the parton gas cools considerably faster than predicted by Bjorken's scaling solution ($T^3\tau = \text{const.}$) shown as dotted lines, because the production of additional partons approaching the chemical equilibrium state consumes an appreciable amount of energy. The accelerated cooling, in

turn, slows down the chemical equilibration process, which is more apparent at RHIC than at LHC energies. Therefore, the parton system can hardly reach its equilibrium state before the effective temperature drops below $T_c \approx 200$ MeV in a short period of time of 1-2 fm/ c at RHIC energy. At LHC energy, however, the parton gas becomes very close to its equilibrium and the plasma may exist in a deconfined phase for as long as 4-5 fm/ c . Another important observation is that quarks never approach to chemical equilibrium at both energies. This is partially due to the small initial quark fugacity and partially due to the small quark equilibration rate.

We note that the initial conditions used here result from the HIJING model calculation in which only initial direct parton scatterings are taken into account. Due to the fact that HIJING is a pQCD motivated phenomenological model, there are some uncertainties related to the initial parton production, as listed in Ref. [7]. We can estimate the effect of the uncertainties in the initial conditions on the parton gas evolution by multiplying the initial energy and parton number densities at RHIC energy by a factor of 4. This will result in the initial fugacities, $\lambda_g^0 = 0.2$ and $\lambda_q^0 = 0.024$. With these high initial densities, the parton plasma can evolve into a nearly equilibrated gluon gas as shown in Fig. 4. The deconfined phase will also last longer for about 4 fm/ c . Though, the system is still dominated by gluons with few quarks and antiquarks as compared to a fully chemical equilibrated system. If the uncertainties in the initial conditions are caused by the soft parton production from the color mean fields, the initial effective temperature will decrease. Therefore, we can alternatively increase the initial parton density by a factor of 4 and decrease T_0 to 0.4 GeV at the same time. This leads to higher initial fugacities, $\lambda_g^0 = 0.52$ and $\lambda_q^0 = 0.083$. As shown in Fig. 4 by the curves with stars, this system evolves faster toward equilibrium, however, with shorter life-time in the deconfined phase due to the reduced initial temperature.

We thus can conclude that perturbative parton production and scatterings are very likely to produce a quark-gluon plasma (or more specifically a gluon plasma) in ultrarelativistic heavy ion collisions at LHC energy. However, the fate of the quark-gluon plasma at RHIC energy has to be determined by a more careful examination of the uncertainties in the

initial conditions. These uncertainties will surely affect the open charm production during the equilibration as we shall discuss.

III. THERMAL CHARM PRODUCTION DURING EQUILIBRATION

With the given evolution of the parton gas, we can now calculate open charm production during the parton equilibration. Similar to light quarks, charm quarks are produced through gluon fusion $gg \rightarrow c\bar{c}$ and quark antiquark annihilation $q\bar{q} \rightarrow c\bar{c}$ during the evolution of the parton plasma. However, since the number of charm quarks is very small as compared to gluons and light quarks, we can neglect the back reactions, $c\bar{c} \rightarrow gg$, $q\bar{q}$ and their effect on the parton evolution. Given the phase-space density of the equilibrating partons, $f_i(k)$, the differential production rate is [9],

$$E \frac{d^3 A}{d^3 p} = \frac{1}{16(2\pi)^8} \int \frac{d^3 k_1}{\omega_1} \frac{d^3 k_2}{\omega_2} \frac{d^3 p_2}{E_2} \delta^{(4)}(k_1 + k_2 - p - p_2) \left[\frac{1}{2} g_G^2 f_g(k_1) f_g(k_2) |\overline{\mathcal{M}}_{gg \rightarrow c\bar{c}}|^2 + g_q^2 f_q(k_1) f_{\bar{q}}(k_2) |\overline{\mathcal{M}}_{q\bar{q} \rightarrow c\bar{c}}|^2 \right], \quad (25)$$

where $g_G=16$, $g_q = 6N_f$, are the degeneracy factors for gluons and quarks (antiquarks) respectively, $|\overline{\mathcal{M}}_{gg \rightarrow c\bar{c}}|^2$, $|\overline{\mathcal{M}}_{q\bar{q} \rightarrow c\bar{c}}|^2$ are the *averaged* matrix elements for $gg \rightarrow c\bar{c}$ and $q\bar{q} \rightarrow c\bar{c}$ processes, respectively,

$$\begin{aligned} \frac{|\overline{\mathcal{M}}_{gg \rightarrow c\bar{c}}|^2}{\pi^2 \alpha_s^2} &= \frac{12}{\hat{s}^2} (M^2 - \hat{t})(M^2 - \hat{u}) + \frac{8}{3} \left(\frac{M^2 - \hat{u}}{M^2 - \hat{t}} + \frac{M^2 - \hat{t}}{M^2 - \hat{u}} \right) \\ &\quad - \frac{16M^2}{3} \left[\frac{M^2 + \hat{t}}{(M^2 - \hat{t})^2} + \frac{M^2 + \hat{u}}{(M^2 - \hat{u})^2} \right] - \frac{6}{\hat{s}} (2M^2 - \hat{t} - \hat{u}) \\ &\quad + \frac{6}{\hat{s}} \frac{M^2(\hat{t} - \hat{u})^2}{(M^2 - \hat{t})(M^2 - \hat{u})} - \frac{2}{3} \frac{M^2(\hat{s} - 4M^2)}{(M^2 - \hat{t})(M^2 - \hat{u})}, \end{aligned} \quad (26)$$

$$\frac{|\overline{\mathcal{M}}_{q\bar{q} \rightarrow c\bar{c}}|^2}{\pi^2 \alpha_s^2} = \frac{64}{9\hat{s}^2} \left[(M^2 - \hat{t})^2 + (M^2 - \hat{u})^2 + 2M^2\hat{s} \right], \quad (27)$$

Due to the small charm density, we can neglect the Pauli blocking of the final charm quarks. For large charm quark mass, M , we can approximate the phase-space density $f_i(k)$ by a Boltzmann distribution. We further assume that the distributions are boost invariant, *i.e.*,

$$f_i(k) \approx \lambda_i e^{-k_\perp \cosh(y-\eta)}, \quad (28)$$

where $\eta = 0.5 \ln(t+z)/(t-z)$ is the spatial rapidity of a space-time cell at (t, z) . Neglecting the transverse expansion, the above assumption implies that the space-time cell at (t, z) have a flow velocity, $u = (\cosh \eta, \sinh \eta)$. We can now complete the integral over η in $\int d^4x = \pi R_A^2 \int d\eta d\tau$ and obtain,

$$\frac{dN_{\text{th}}}{dy d^2p_{\perp}} = \frac{\pi R_A^2}{16(2\pi)^8} \int_{\tau_{\text{iso}}}^{\tau_c} \tau d\tau \int p_{\perp 2} dp_{\perp 2} d\phi_2 dy_2 d\phi_{k1} dy_{k1} \frac{2k_{\perp 1}^2}{\hat{s}} 2K_0(Q_{\perp}/T) \left[\frac{1}{2} g_G^2 \lambda_g^2 |\overline{\mathcal{M}}_{gg \rightarrow c\bar{c}}|^2 + g_q^2 \lambda_q^2 |\overline{\mathcal{M}}_{q\bar{q} \rightarrow c\bar{c}}|^2 \right], \quad (29)$$

where K_0 is the modified Bassel function and τ_c is the time when the temperature, T , drops below 200 MeV. The kinematic variables are chosen such that,

$$p_2 = (M_{\perp 2} \cosh y_2, p_{\perp 2} \cos \phi_2, p_{\perp 2} \sin \phi_2, M_{\perp 2} \sinh y_2), \quad M_{\perp 2} = \sqrt{M^2 + p_{\perp 2}^2}; \\ k_i = k_{\perp i} (\cosh y_{ki}, \cos \phi_{ki}, \sin \phi_{ki}, \sinh y_{ki}), \quad i = 1, 2. \quad (30)$$

The center-of-mass momentum, $Q = (Q_{\perp} \cosh y_Q, \mathbf{q}_{\perp}, Q_{\perp} \sinh y_Q)$, is defined as $Q = p + p_2 = k_1 + k_2$, and

$$Q^2 = \hat{s} = 2[M^2 + M_T M_{\perp 2} \cosh(y - y_2) - p_{\perp} p_{\perp 2} \cos \phi_2], \\ q_{\perp}^2 = p_{\perp}^2 + p_{\perp 2}^2 + 2p_{\perp} p_{\perp 2} \cos \phi_2, \\ Q_{\perp}^2 = Q^2 + q_{\perp}^2 = M_T^2 + M_{\perp 2}^2 + 2M_T M_{\perp 2} \cosh(y - y_2). \quad (31)$$

Using these variables and the energy-momentum conservation, we have,

$$k_{\perp 1} = \frac{Q^2/2}{M_{\perp} \cosh(y - y_{k1}) + M_{\perp 2} \cosh(y_2 - y_{k1}) - q_{\perp} \cos \phi_{1q}}, \\ \cos \phi_{1q} = [p_{\perp} \cos \phi_{k1} + p_{\perp 2} \cos(\phi_2 - \phi_{k1})]/q_{\perp}. \quad (32)$$

In the integral over τ , we shall use the time evolution of the temperature, $T(\tau)$, and fugacities, $\lambda_i(\tau)$, as given in the previous section.

IV. PRE-THERMAL CHARM PRODUCTION

Before the parton distributions reach local isotropy in momentum space so that the rate equations can be applied to describe the equilibration of the parton system, scatterings

among free-streaming partons can also lead to charm production. Since the system during this period consists dominantly of gluons, we shall only consider gluon fusions. To model the phase-space distribution, we take into account the distribution of the initial production points which spread over a region of width,

$$\Delta_k \approx \frac{2}{k_\perp \cosh y}, \quad (33)$$

in z coordinate. Following Ref. [11], we assume free-streaming until τ_{iso} and neglect the expansion in the transverse direction. The correlated phase-space distribution function is given by

$$f(k, x) = \frac{1}{g_G \pi R_A^2} g(k_\perp, y) \frac{e^{-(z-t \tanh y)^2/2\Delta_k^2}}{\sqrt{2\pi}\Delta_k} \theta(R_A - r) \theta(\tau_{\text{iso}} \cosh y - t), \quad (34)$$

where $g(k_\perp, y)$ is the parametrization of the parton spectrum given by HIJING simulations,

$$g(k_\perp, y) = \frac{(2\pi)^3}{k} \frac{dN_g}{dy d^2 k_\perp} = \frac{(2\pi)^2}{k} h(k_\perp) \frac{1}{2Y} \theta(Y^2 - y^2). \quad (35)$$

The phase-space distribution is normalized such that $\lim_{t \rightarrow \infty} g_G \int d^3 x f(k, x) / (2\pi)^3 = d^3 N_g / d^3 k$. The function $h(k_\perp)$ and the rapidity width Y are given in Table II for central $Au + Au$ collisions at RHIC and LHC energies which also gives the initial conditions as listed in Table I.

Substituting the phase-space distribution, into Eq. (25), and integrate over space and time, we obtain the charm production distribution in the pre-thermal period,

$$\frac{dN_{\text{pre}}}{dy d^2 p_\perp} = \frac{1}{16(2\pi)^8 \pi R_A^2} \int p_{\perp 2} dp_{\perp 2} d\phi_2 dy_2 d\phi_{k1} dy_{k1} \frac{2k_{\perp 1}^2}{\hat{s}} g(k_{\perp 1}, y_{k1}) g(k_{\perp 2}, y_{k2}) \frac{1}{2} |\overline{\mathcal{M}}_{gg \rightarrow cc}|^2 \frac{1}{\sqrt{2\pi}\Delta_{\text{tot}}} \int_0^{t_f} dt e^{-t^2(\tanh y_1 - \tanh y_2)^2/2\Delta_{\text{tot}}^2}, \quad (36)$$

$$\Delta_{\text{tot}} = \sqrt{\Delta_{k1}^2 + \Delta_{k2}^2}, \quad t_f = \tau_{\text{iso}} \min(\cosh y_{k1}, \cosh y_{k2}). \quad (37)$$

where the kinematic variables are similarly defined as in Eq. (29), and in addition,

$$\begin{aligned} k_{\perp 2}^2 &= Q_\perp^2 + k_{\perp 1}^2 - 2k_{\perp 1} [M_\perp \cosh(y - y_{k1}) + M_{\perp 2} \cosh(y_2 - y_{k1})], \\ \sinh y_{k2} &= [M_\perp \sinh y + M_{\perp 2} \sinh y_2 - k_{\perp 1} \sinh y_{k1}] / k_{\perp 2}. \end{aligned} \quad (38)$$

Note that the correlation between momentum and space-time in the phase-space distribution was not considered in a previous calculation [9]. As we will show this correlation is very important and will reduce the pre-thermal charm production as compared to the uncorrelated distributions. Similar effect was recently discussed by Lin and Gyulassy in Ref. [11], where formation time effect is also included which is expected to further suppress pre-thermal charm production.

V. INITIAL FUSION

During the initial interaction period, charm quarks are produced together with minijets through gluon fusion and quark anti-quark annihilation. Like gluon and light quark production, charm production through the initial fusion is very sensitive to the parton distributions inside nuclei. In addition, the cross section is also very sensitive to the value of charm quark mass, M . If higher order corrections are taken into account, the production cross section depends also on the choices of the renormalization and factorization scales. Detailed studies on the next-leading-order calculation [31–34] shows, however, that higher order corrections to the total charm production cross section can be accounted for by a constant K -factor of about 2. This is what we will use next. For consistency we use $M = 1.5$ GeV for all calculations. Shown in Figs. 5 and 6 as solid lines are the initial charm production given by HIJING calculations at RHIC and LHC energies, with MRSD–' [35] parton distributions. The corresponding total integrated cross sections are, $\sigma_{c\bar{c}} = 0.16$ (5.75) mb at RHIC (LHC) energy, where nuclear shadowing of the gluon distribution function is also taken into account. In HIJING calculations, high order corrections are included via parton cascade in both initial and final state radiations. The resultant distributions in $c\bar{c}$ -pair momentum are very close to the explicit higher order calculations [34].

Plotted in Figs. 5 and 6 as dot-dashed and dashed lines are the pre-thermal and thermal production. In the calculation, a factor of 2 is also multiplied to the lowest order matrix elements of charm production. Both contributions are much smaller than the initial charm

production at both energies. The pre-thermal contributions shown are also much smaller than what was found in Ref. [9]. This is because momentum and space-time correlation was not taken into account in Ref. [9] which suppresses the pre-thermal charm production. Similar results are also found in a study by Lin and Gyulassy [11]. As we have already discussed, the initial conditions in Tables I and II given by HIJING calculations have many uncertainties. If one increases the initial parton number density at RHIC energy by a factor of 4 with the same initial temperature, charm production from both pre-thermal and thermal sources will increase about a factor of 12 as shown in Fig. 7, leading to a total secondary contribution comparable to the initial charm production. In the extreme limit, a fully equilibrated parton plasma ($\lambda_g = \lambda_q = 1$) at the same initial temperature would give an enhancement of charm production about 4 times higher than the initial production, shown as dotted lines in Figs. 5 and 6. In this case, the enhancement not only comes from higher parton densities, but also from the much longer life time of the parton plasma (cf. Figs. 2 and 3). Much higher enhancements predicted in Ref. [10] are due to the overestimate of the intrinsic charm production as pointed by Gyulassy and Lin in a recent paper [11]. Though the intrinsic charm production is important in the forward direction at large x_f [36], it is strongly suppressed in the mid-rapidity region due to the interference among pQCD amplitudes to the same order [37].

To test the sensitivity of open charm production to uncertainties in initial fugacities and temperature separately, we consider an alternative scenario as we have discussed in the parton evolution. We assume the initial parton densities to be 4 times higher than given in Table I at RHIC energy but with lower initial temperature, $T_0 = 0.4$ GeV. Accordingly, the initial phase-space distribution is also modified to: $h(k_\perp) = 9649.2e^{-k_\perp/0.65}/(k_\perp + 0.3)$ from the one in Table II, which gives 4 times of the initial parton density but smaller average transverse momentum, $\langle k_\perp \rangle = 0.85$ GeV. The reduced average transverse momentum corresponds to lower initial effective temperature. This system with higher initial fugacities evolves faster toward equilibrium but the life-time of the deconfined phase is shorter due to the reduced temperature as we have discussed. The corresponding open charm production

is shown in Fig. 7 by the lines with stars. We observe that open charm production from both pre-thermal and thermal contribution is reduced due to the reduction in initial temperature and life-time of the parton plasma, even though the initial fugacities are much higher and the evolution toward equilibrium is faster. Thus, open charm production is much more sensitive to the change in the initial temperature than the parton fugacities. We also note from Eqs. (29) and (36) that the pre-thermal and thermal charm production depends on the thermalization time τ_{iso} and the life time of the parton plasma. Therefore, by measuring the charm enhancement, we can probe the initial parton phase-space distribution, initial temperature and the thermalization and equilibration time.

VI. CONCLUSIONS

In this paper, we have calculated open charm production in an equilibrating parton plasma, taking into account the evolution of the effective temperature and parton fugacities according to the solution of a set of rate equations. In the evaluation of the interaction rate R_3 for induced gluon radiation, a color dependent effective formation time was used which reduces the gluon equilibration rate through LPM suppression of soft gluons. In the calculation of the pre-thermal contribution to open charm production, correlation between momentum and space-time was also included. This correlation reduces the pre-thermal charm production as compared to the uncorrelated one used in a previous estimate [9].

We found that both the thermal contribution during the parton equilibration and pre-thermal contribution with the current estimate of the initial parton density from HIJING Monte Carlo simulation are much smaller than the initial direct charm production. However, the final total charm production is very sensitive to the initial condition of the parton evolution. If uncertainties in the initial parton production can increase the initial parton density, *e.g.*, by a factor of 4, the total secondary charm production will become comparable or larger than the initial production, due to both the increased production rate and longer life time of the parton plasma. We also found that open charm production is more sensitive

to the initial temperature of the parton system than the initial parton fugacities. Therefore, open charm production is a good probe of the initial parton distribution in phase-space and the thermalizaion and equilibration time of the parton plasma.

ACKNOWLEDGMENTS

P. L. and X.-N. W. would like to thank M. Asakawa and M. Gyulassy for helpful discussions. B. M. and X.-N. W. thank T. S. Birò, E. van Doorn, and M. H. Thoma for their early collaboration in the study of parton equilibration. This work was supported by the Director, Office of Energy Research, Division of Nuclear Physics of the Office of High Energy and Nuclear Physics of the U.S. Department of Energy under Contract No. DE-AC03-76SF00098 and DE-FG05-90ER40592. P. L. and X.-N. W. were also supported by the U.S. - Hungary Science and Technology Joint Fund J. F. No. 378.

REFERENCES

- [1] X.-N. Wang and M. Gyulassy, Phys. Rev. D **44**, 3501 (1991); Comp. Phys. Commun. (1994), in press.
- [2] K. Geiger and B. Müller, Nucl. Phys. **B369**, 600 (1992); K. Geiger, Phys. Rev. D **47**, 133 (1993).
- [3] H. J. Moehring and J. Ranft, Z. Phys. C **52**, 643 (1991); P. Aurenche, *et al.*, Phys. Rev. D **45**, 92 (1992). P. Aurenche, *et al.*, Comp. Phys. Commun. **83**, 107 (1994).
- [4] J.P. Blaizot, A.H. Mueller, Nucl. Phys. **B289**, 847 (1987).
- [5] K. Kajantie, P. V. Landshoff and J. Lindfors, Phys. Rev. Lett. **59**, 2517 (1987); K. J. Eskola, K. Kajantie and J. Lindfors, Nucl. Phys. **B323**, 37 (1989); K. J. Eskola, K. Kajantie and J. Lindfors, Phys. Lett. B **214**, 613 (1989).
- [6] E. Shuryak, Phys. Rev. Lett. **68**, 3270 (1992).
- [7] T. S. Biró, E. van Doorn, B. Müller, M. H. Thoma, and X.-N. Wang, Phys. Rev. C **48**, 1275 (1993).
- [8] L. Xiong and E. Shuryak, Phys. Rev. C **49**, 2207 (1994).
- [9] B. Müller and X.-N. Wang, Phys. Rev. Lett. **68**, 2437 (1992).
- [10] K. Geiger, Phys. Rev. D **48**, 4129 (1993).
- [11] Z. Lin and M. Gyulassy, CU-TP-638, nucl-th-9409007.
- [12] E. Shuryak and L. Xiong, Phys. Rev. Lett. **70**, 2241 (1993).
- [13] M. T. Strickland, Phys. Lett. B **331**, 245 (1994).
- [14] X.-N. Wang, in proceedings of the Workshop on Finite Temperature QCD and Quark-gluon Transport Theory, Wuhan, China, April 18-26, 1994, edited by Lianshou Liu (World Scientific).

- [15] P. B. Straub *et al.*, Phys. Rev. Lett. **68**, 452 (1992).
- [16] S. J. Brodsky and H. J. Lu, Phys. Rev. Lett. **64**, 1342 (1990).
- [17] K. J. Eskola, J. Qiu and X.-N. Wang, Phys. Rev. Lett. **72**, 36 (1994).
- [18] X.-N. Wang and M. Gyulassy, Phys. Rev. Lett. **68**, 1480 (1992).
- [19] K. J. Eskola and X.-N. Wang, Phys. Rev. D **49**, 1284 (1994).
- [20] M. Gyulassy and X.-N. Wang, Nucl. Phys. B **420**, 583 (1994).
- [21] X.-N. Wang, M. Gyulassy and M. Plúmer, LBL-35980, hep-ph/9408344.
- [22] T. S. Biró, B. Müller, and X.-N. Wang, Phys. Lett. **B283**, 171 (1992).
- [23] B. Andersson, G. Gustafson, G. Ingelman and T. Sjöstrand, Phys. Rep. **97**, 31 (1983).
- [24] K. J. Eskola and M. Gyulassy, Phys. C **47**, 2329 (1993).
- [25] T. Matsui, B. Svetitsky, and L. McLerran, Phys. Rev. D **34**, 783 (1986).
- [26] P. Danielewicz and M. Gyulassy, Phys. Rev. D **31**, 53 (1985); A. Hosoya and K. Kajantie, Nucl. Phys. **B250**, 666 (1985); S. Gavin, Nucl. Phys. **A435**, 826 (1985).
- [27] J. D. Bjorken, Phys. Rev. D **27**, 140 (1983).
- [28] E. Braaten and R. D. Pisarski, Nucl. Phys. **B337**, 569 (1990).
- [29] T. S. Biró and B. Müller, Nucl. Phys. **A561**, 477 (1993).
- [30] J. F. Gunion and G. Bertsch, Phys. Rev. D **25**, 746 (1982).
- [31] P. Nason, S. Dawson, and R.K. Ellis, Nucl. Phys. **B303**, 607 (1988); *ibid.* **B327**, 49 (1989); M.L. Mangano, P. Nason, and G. Ridolfi, Nucl. Phys. **B373**, 295 (1992).
- [32] W. Beenakker, H. Kuijf, W.L. van Neerven, and J. Smith, Phys. Rev. **D40**, 54 (1989); W. Beenakker, W.L. van Neerven, R. Meng, G.A. Schuler, and J. Smith, Nucl. Phys. **B351**, 507 (1991).

- [33] I. Sarcevic and P. Valerio, Phys. Lett. **B338**, 426 (1994); AZPH-TH-94-20, 1994.
- [34] R. Vogt, *et al.*, in Hard Processes in Hadronic Interactions, edited by H. Satz and X.-N. Wang, to be published.
- [35] A. D. Martin, W. J. Striling and R. G. Roberts, Phys. Lett. **306B**, 145 (1993).
- [36] R. Vogt, S. J. Brodsky abd P. Hoyer, Nucl. Phys. *bf* B383, 643 (1992); S. J. Brodsky, P. Hoyer, A. H. Mueller and W. K. Tang, *ibid.* **B 369**, 519 (1992).
- [37] J. C. Collins, D. E. Soper and G. Sterman, Nucl. Phys. **B263**, 37 (1986).

TABLES

	RHIC	LHC
τ_{iso} (fm/c)	0.7	0.5
ε_0 (GeV/fm ³)	3.2	40
n_0 (fm ⁻³)	2.15	18
$\langle k_{\perp} \rangle$ (GeV)	1.17	1.76
T_0 (GeV)	0.55	0.82
λ_g^0	0.05	0.124
λ_q^0	0.008	0.02

TABLE I. Values of the relevant parameters characterizing the parton plasma at the moment τ_{iso} , when local isotropy of the momentum distribution is first reached.

\sqrt{s} (TeV)	Y	$h(k_{\perp})$ (GeV ⁻²)
0.2	2.5	$1754.4e^{-k_{\perp}/0.9}/(k_{\perp} + 0.3)$
5.5	5.0	$2.66 \times 10^7/(k_{\perp} + 2.9)^{6.4}$

TABLE II. Parametrizations of the momentum spectra of the initially produced partons in HIJING calculation.

FIGURES

FIG. 1. The scaled gluon production rate R_3/T (solid line) for $gg \rightarrow ggg$ and the quark production rate R_2/T (dashed line) for $gg \rightarrow q\bar{q}$ are shown as function of the gluon fugacity λ_g for $\alpha_s = 0.3$.

FIG. 2. Time evolution of the temperature T and the fugacities λ_g and λ_q of gluons and quarks in the parton plasma created in Au + Au collisions at the RHIC energy of $\sqrt{s} = 200$ AGeV. The initial values for T , λ_g and λ_q are determined from HIJING simulations and are listed in Table I.

FIG. 3. The same as in Fig. 2, except for LHC energy, $\sqrt{s} = 5.5$ ATeV.

FIG. 4. The same as in Fig. 2, except that the initial parton densities are 4 times higher than given in Table I with the same (ordinary lines), or reduced initial temperature, $T_0 = 0.4$ GeV (lines with stars)

FIG. 5. The p_\perp distributions of initial (solid), prethermal (dot-dashed), and thermal (dashed) charm production for central $Au + Au$ collisions at RHIC energy, $\sqrt{s} = 200$ AGeV with initial conditions given in Tables I and II. The dotted line is the thermal production assuming an initial fully equilibrated QGP at the same temperature.

FIG. 6. The same as in Fig. 5, except at LHC energy, $\sqrt{s} = 5.5$ ATeV.

FIG. 7. The p_\perp distribution of the initial (solid), pre-thermal (dot-dashed) and thermal (dashed) charm production for initial parton densities 4 times higher than HIJING estimate given in I but with the same (ordinary lines), or reduced initial temperature, $T_0 = 0.4$ GeV (lines with stars).

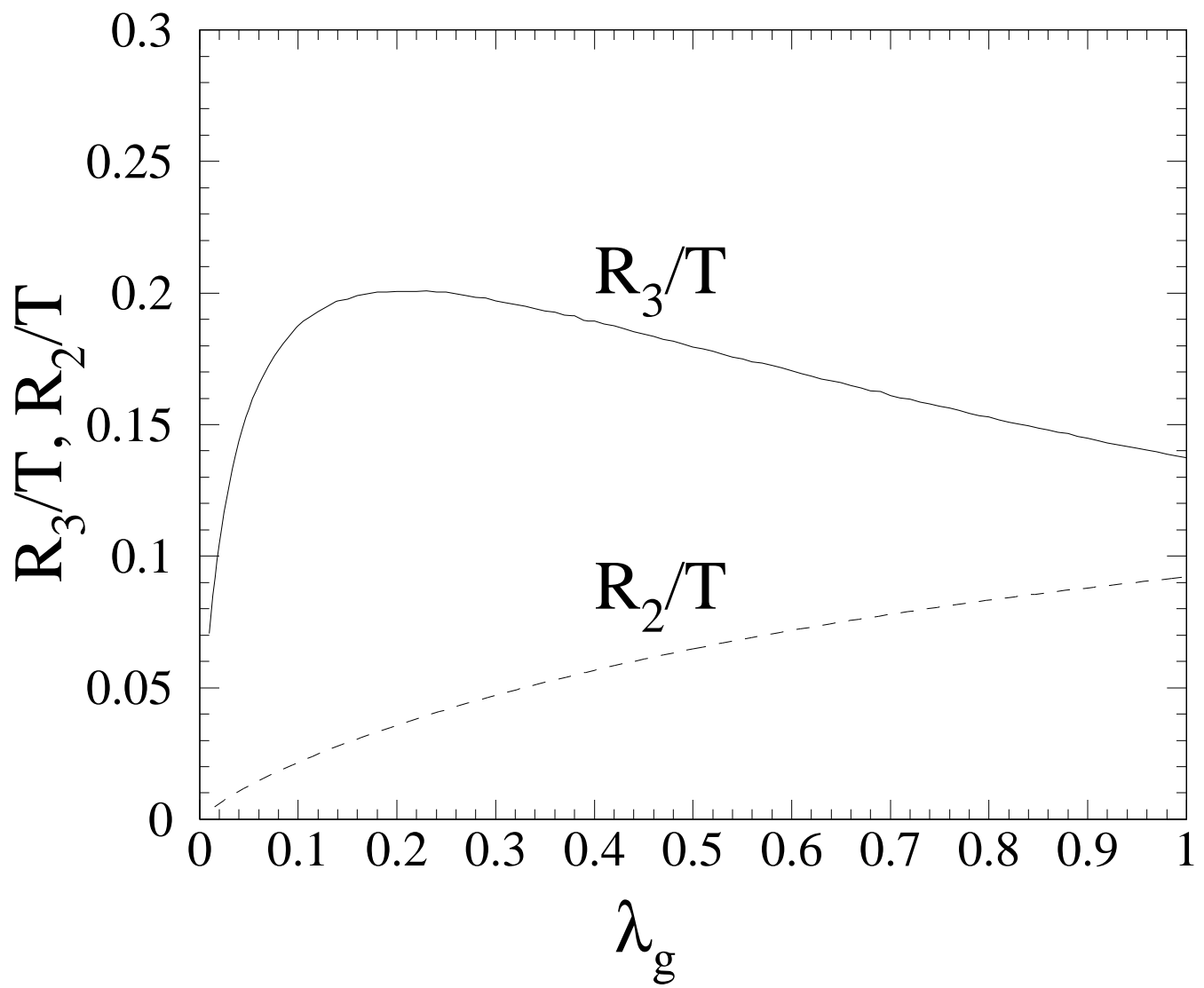


Fig. 1

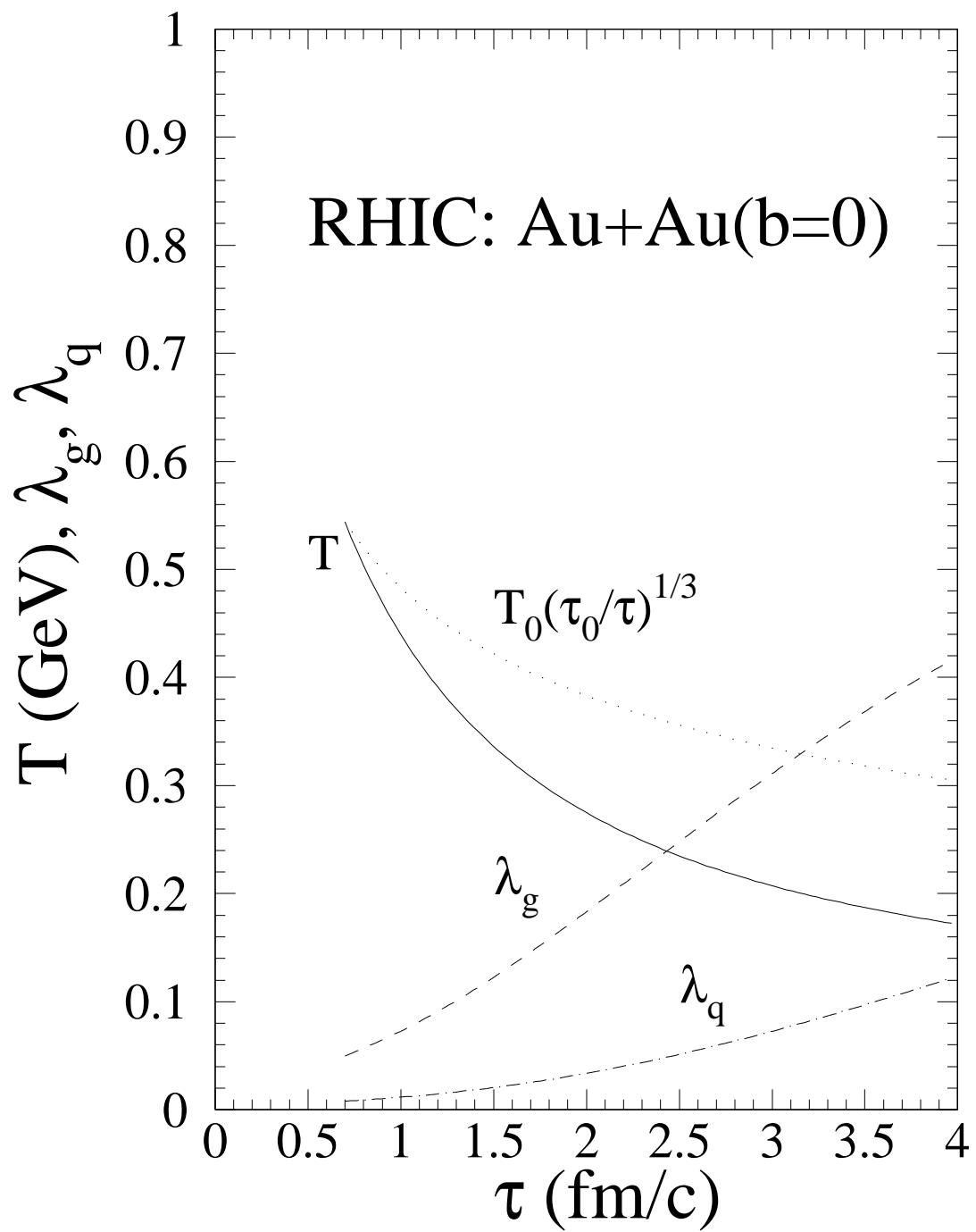


Fig. 2

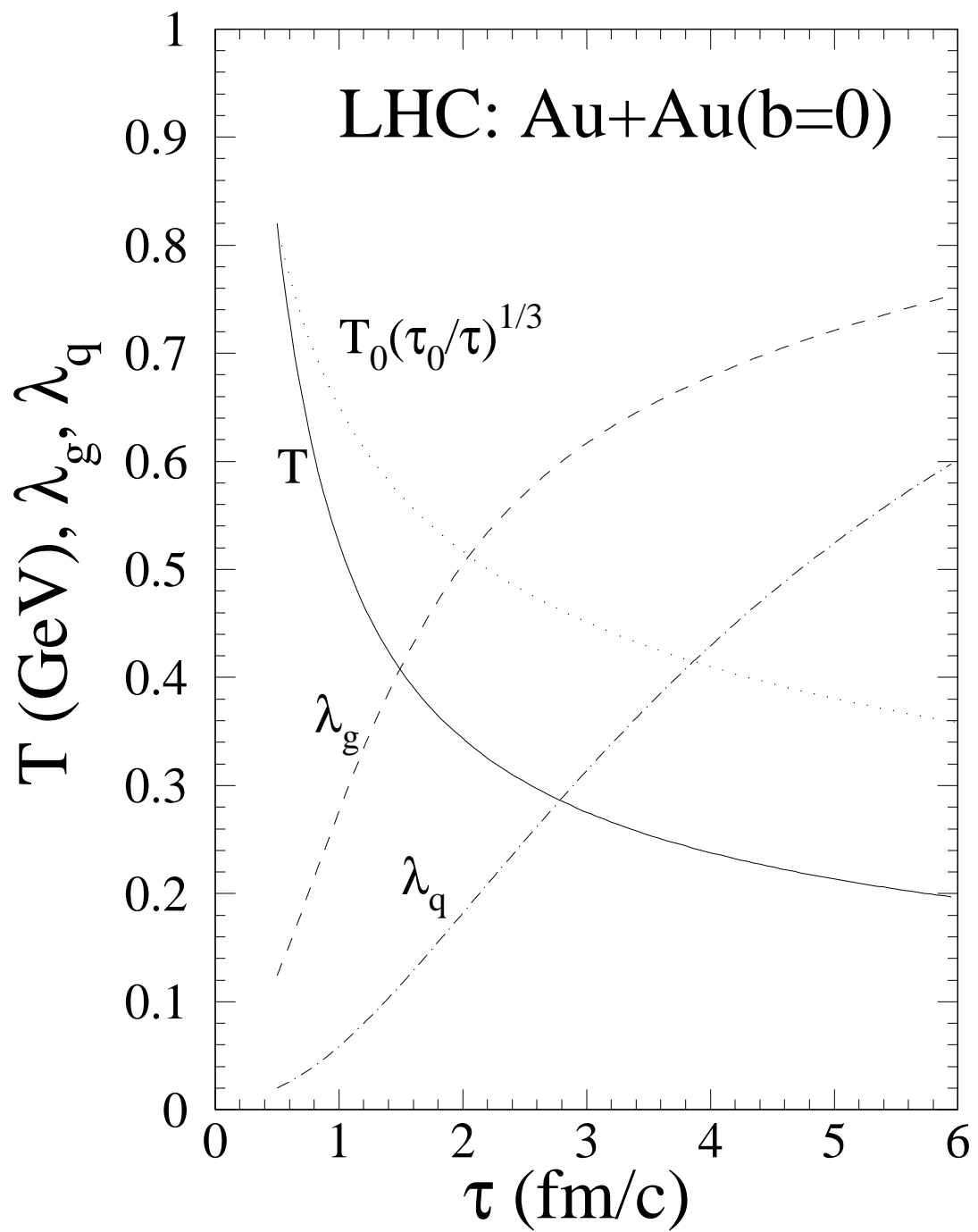


Fig. 3

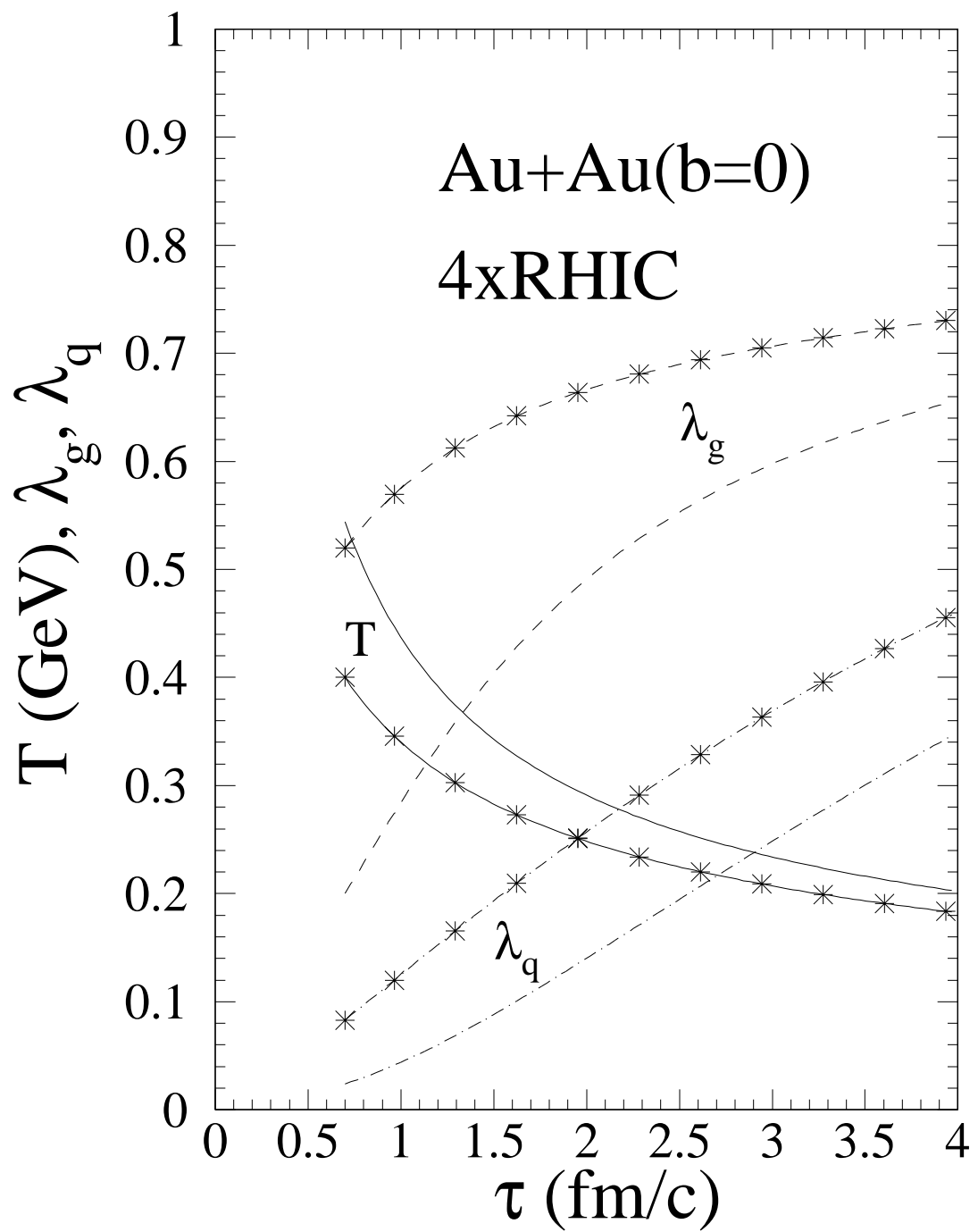


Fig. 4

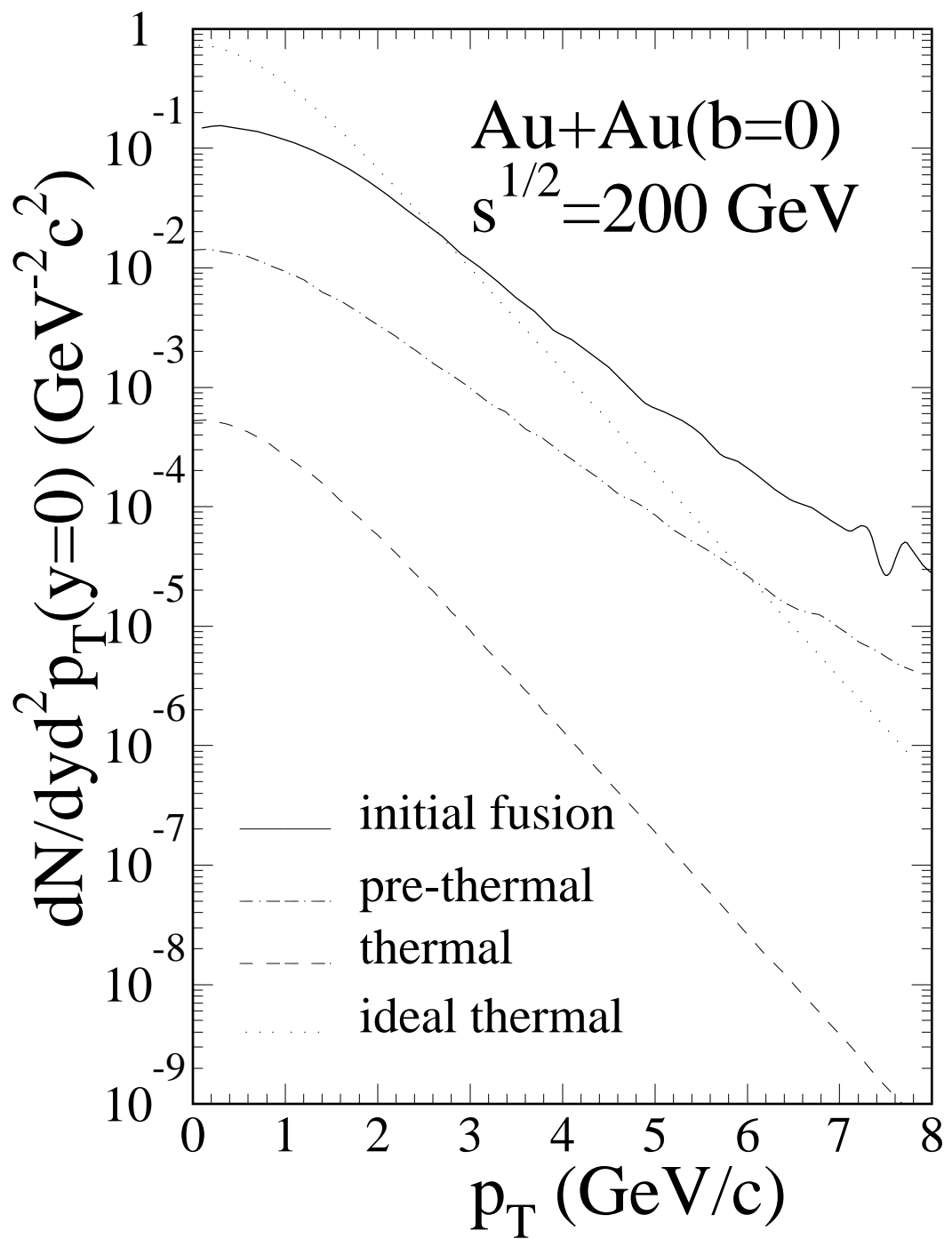


Fig. 5

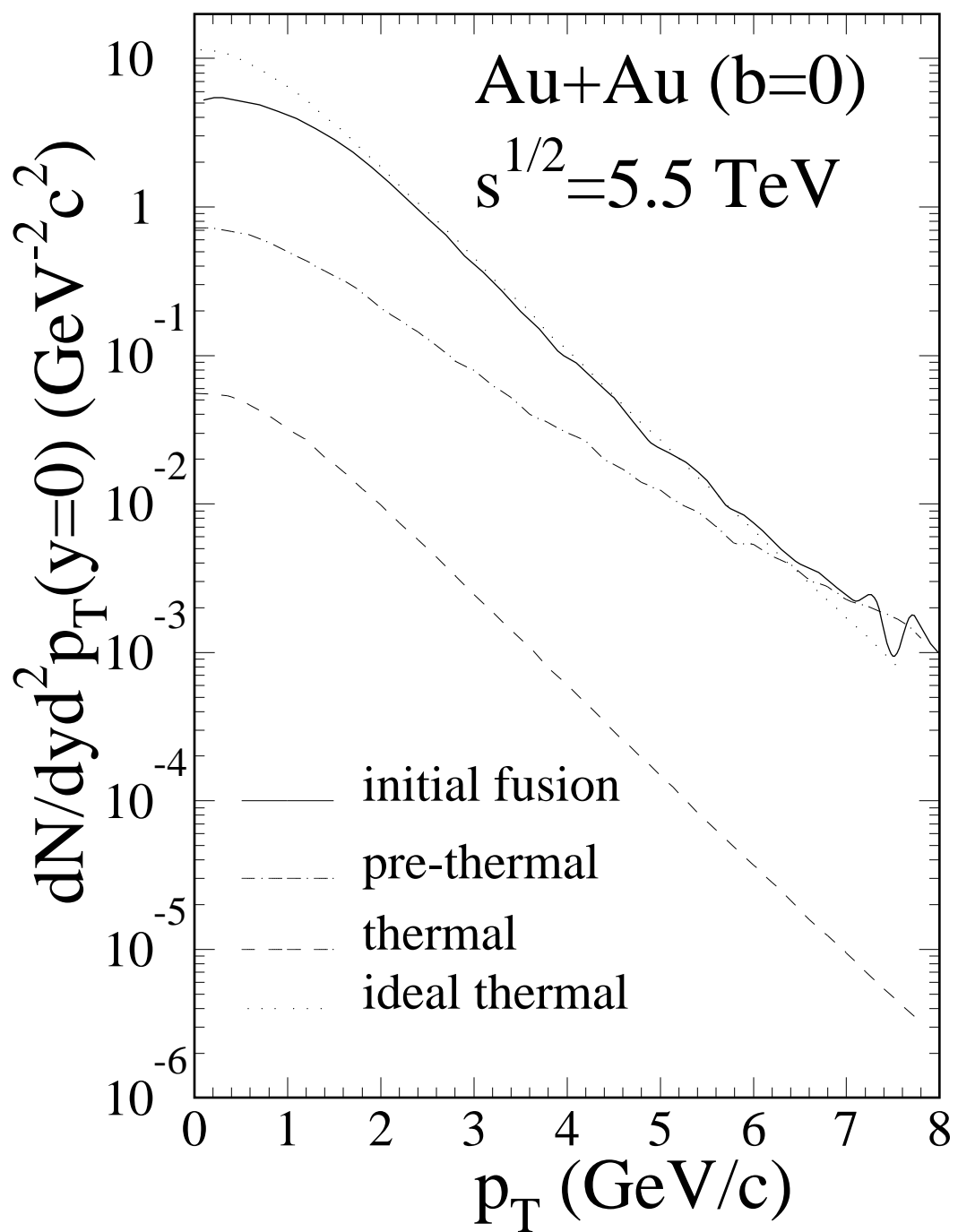


Fig. 6

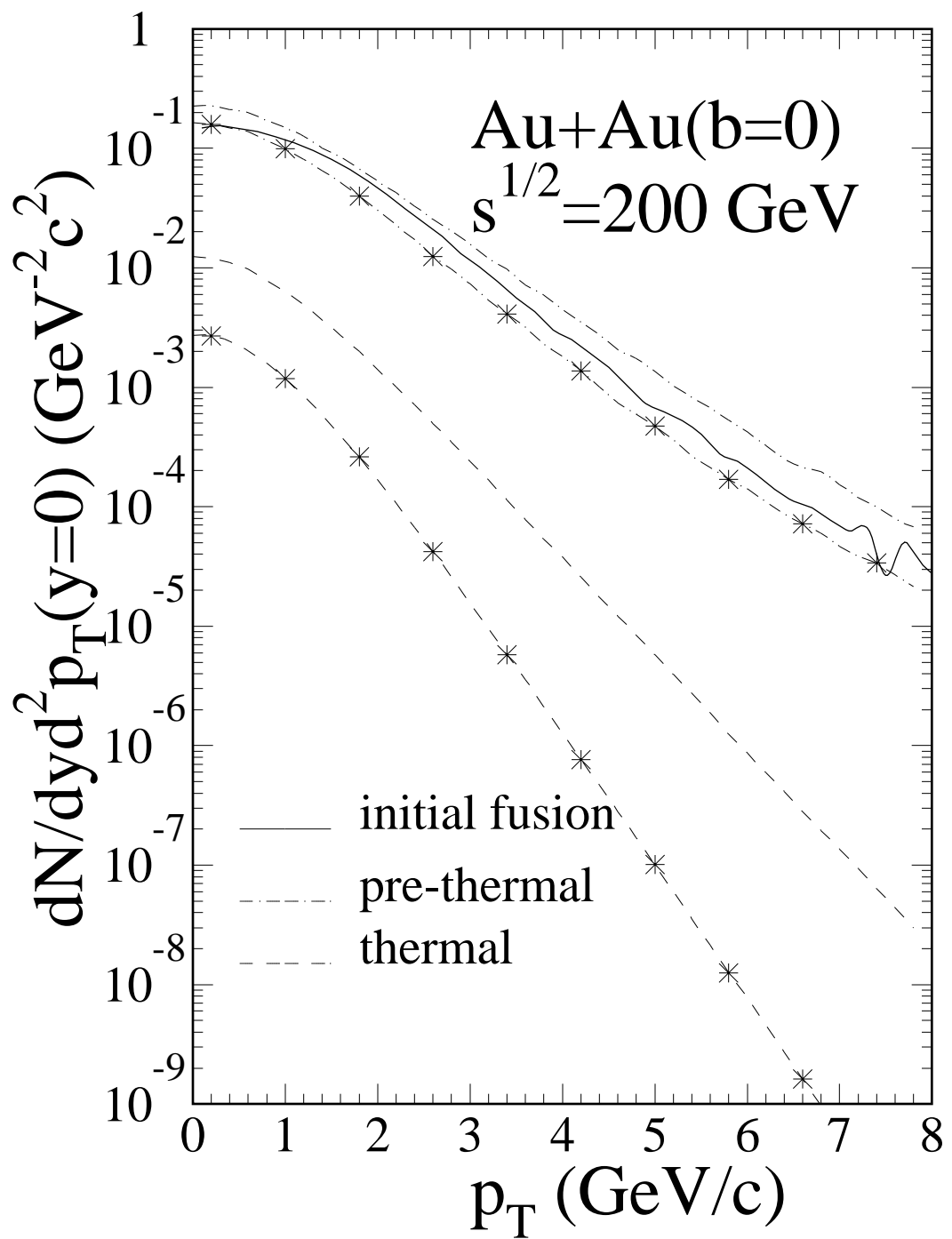


Fig. 7